Human Erythrocyte Ghosts: Exploring the Origins of Multiexponential Water Diffusion in a Model Biological Tissue With Magnetic Resonance

Peter E. Thelwall,[1*] Samuel C. Grant,[1,3] Greg J. Stanisz,[2] and Stephen J. Blackband[1,3]

A tissue model composed of erythrocyte ghosts was developed to study the effects of compartmentation on the MR signal acquired from biological tissues. This simple and flexible model offers control over the biophysical parameters that contribute to multicomponent signals arising from cellular systems. Cell density, size, intra- and extracellular composition, and membrane permeability can be independently altered. The effects of cell density and cell size on water diffusion properties were assessed. The data demonstrate non-monoexponential water diffusion in ghost cell suspensions of 17–67% cell density. Data were analysed with the widely employed two-compartment (biexponential) model, and with a two-compartment model that accounted for exchange between compartments. Water exchange between the intra- and extracellular compartments appeared to be significant over the range of diffusion times studied (7–35 ms). The biexponential fit to the ghost data appeared to be underparameterised as the ADCs and relative fractions of the fast and slow components were dependent on the experimental acquisition parameters, specifically the diffusion time. However, both analysis methods proved effective at tracking changes in the ghost model when it was perturbed. This was demonstrated with cell density variation, cell swelling and shrinkage experiments, and reduction of membrane water permeability using a water channel blocker (pCMBS). We anticipate that this model system could be used to investigate compartmental diffusion effects to simulate a range of pathologies, especially ischemic stroke. Magn Reson Med 48:649–657, 2002. © 2002 Wiley-Liss, Inc.

Key words: water diffusion; erythrocyte ghost; compartmentation; diffusion-weighted imaging; model tissue

Biological tissues are multicompartmental and heterogeneous. Because the constituents of a tissue can differ in their MR properties, the heterogeneity of tissue structure can be probed by MR. Biological tissues are composed of vascular, extracellular, cellular, and subcellular compartments. In an MR image of a biological system the signal originates from water molecules in all of these compartments; it is affected by the MR properties of each compartment, and mediated by water exchange between compartments. A change in the MR properties of one or more of these compartments in a tissue can indicate pathology, an example being the rapid decrease in the apparent diffusion coefficient (ADC) of water in brain tissue affected by cerebral ischemia. The biophysical changes that cause this observed change are still being discussed, more than 10 years after the first observation of the effect (1–6). The change is most commonly attributed to ischemic cell swelling increasing the fraction of water with low ADC (3,7); however, studies have suggested that cessation of intracellular transport mechanisms, such as cytoplasmic streaming, may contribute in part to the ADC change (5). Theoretical models have been developed to describe compartmental effects on water diffusion (4,8–10), yet our understanding of the effects of tissue structure and microstructure on water diffusion remains incomplete. The common goal of research in this field is to comprehend the observed changes in clinical MRI in terms of tissue structure, and relate this change to tissue function in a quantitative manner. It is anticipated that this systematic approach will lead to an improvement in the clinical specificity and sensitivity of MRI, thus improving its diagnostic capabilities in a variety of disease states.

Heavily diffusion-weighted (high b-value) MRI has demonstrated that water diffusion in biological tissues is non-monoexponential, as observed in isolated rat brain (6) and heart (11–13) slices, bovine optic nerve (10,14) and muscle (15), rat brain in vivo (3), and human brain in clinical experiments (16,17). Previous studies on isolated rat brain slices suggested that the fast- and slow-diffusing water components might grossly correspond to extra- and intracellular compartments. This interpretation was used to account for changes in the water diffusion profile on tissue microstructure perturbation caused by physiological insult (6,12,13). This approach is simplistic, however, and more than two compartments may be required. Simulations by other groups imply that more compartments and other factors such as membrane permeability to water and restricted diffusion may be important (4,10,18). In addition, recent studies have suggested that situation may be even more complicated, in that water diffusion in the cytoplasm of a single isolated *Aplysia* neuron is non-monoexponential (19). Some studies have analysed diffusion data by fitting to a continuous distribution of diffusion coefficients, rather than two or three discrete components (20). Similar to a continuous distribution analysis of T_2 data, it has been suggested that this approach may provide a more appropriate representation of water diffusion in a tissue.

In vivo water diffusion studies are hindered by the complexity of the systems under investigation, and the SNR and gradient limitations of the MR technique. As a result, models and model testing procedures (such as perturba-

[1]Department of Neuroscience, McKnight Brain Institute, University of Florida, Gainesville, Florida.
[2]Department of Medical Biophysics, Sunnybrook and Women's College, Health Sciences Center, University of Toronto, Toronto, Canada.
[3]National High Magnetic Field Laboratory, Tallahassee, Florida.
*Correspondence to: Peter E. Thelwall, Ph.D., Department of Neuroscience, Box 100244, Gainesville, FL 32610-0244. E-mail: thelwall@mbi.ufl.edu

tion studies) are required to interpret the data. High-performance MR techniques and hardware are necessary, such as high-quality gradients to allow short diffusion times, so that compartmental exchange issues can be addressed. The aim of the present work was to devise a relatively simple model tissue to study the individual parameters that may affect the observed ADC, T_2, or T_1 of the MR signal acquired from a biological sample. The tissue model described is composed of erythrocyte ghosts, chosen for their simple structure and ease of manipulation. The cell density can be accurately determined and cell size can be varied by changing the osmolarity of the extracellular medium. Furthermore, the ghosts can be resealed to contain molecules of choice, such as proteins or polysaccharides, shift reagents, or T_1 and T_2 relaxation agents, so the constituents of both the intra- and extracellular compartments may be controlled. Membrane permeability to water can be modulated—for example, with the water channel blocker pCMBS (21).

In this study we chose to assess the effects of tissue compartmentalisation on the diffusion properties of water in the erythrocyte ghost model, investigating the effects of changing cell density and cell size on the water diffusion profile. These parameters were chosen because cell swelling is attributed to be the primary cause of contrast in diffusion-weighted imaging (DWI) detection of stroke infarcts (3). The effects of cell density on the ADC of water have been used to monitor cell density (and as a result, malignancy) in in vivo tumour models (22,23). In a preliminary fashion, the data are then fitted by two mathematical approaches to demonstrate the utility of the ghost model for aiding in the development of more complex (and, it is hoped, more appropriate) fitting procedures.

MATERIALS AND METHODS

Erythrocyte Ghost Preparation

Reagents were obtained from Sigma (St. Louis, MO) unless otherwise stated in the text. Human blood was obtained from the left cephalic vein of a healthy volunteer by venipuncture, using ETDA-anticoagulant vacutainer tubes. The study was approved by the University of Florida Institutional Review Board. The blood was centrifuged at $3000 \times g$ for 5 min, and the plasma and buffy coat were discarded. Erythrocytes were washed and centrifuged three times in an isotonic wash buffer (146 mM NaCl, 20 mM HEPES, pH 7.6). Erythrocyte ghosts were prepared by a gel filtration method, as described by Wood (24). A water-jacketed column was packed with agarose gel (A-50 m, 50–100 mesh size; BioRad), and equilibrated with a hypotonic solution to induce haemolysis (5 mM MgSO$_4$, 5 mM KCl, 5 mM PIPES, pH 6.5). Column temperature was maintained at 1–3°C throughout the ghost preparation procedure. A 30–40-cm hydrostatic head was used to load cell suspensions and pass elutant solutions through the column.

A 15% erythrocyte suspension (10 mL) was loaded onto the column, following 10 mL of isotonic wash buffer, which provided for erythrocyte temperature equilibration on the column. The column was then eluted with isotonic wash buffer. The haemolytic erythrocyte ghost membranes passed rapidly through the column, whereas haemoglobin travelled slowly. Eluted ghosts were collected and resealed by incubation at 37°C for 30 min after restoration of isotonicity (addition of a 10% volume of 3M KCl). Ghosts were centrifuged at $12000 \times g$ for 15 min and then resuspended in isotonic wash buffer to approximately 20% cell density. At this stage the ghost suspension had a slight pink colouration, indicating that a small quantity of haemoglobin remained in the ghosts. This was attributed to incomplete separation of ghosts from haemoglobin, resulting in trapping of haemoglobin when the ghosts were resealed. To effect complete removal of haemoglobin, ghost suspensions were passed through the gel filtration column a second time; on elution the ghost suspension was translucent white in appearance, and free from visible contamination by haemoglobin. Ghosts were resealed again and washed by centrifugation at $12000 \times g$ for 15 min, followed by resuspension in isotonic buffered erythrocyte suspension (IBES) solution (125 mM NaCl, 5 mM HEPES, 4.5 mM KCl, 2.5 mM CaCl$_2$, 1.8 mM MgSO$_4$, 5 mM NaHPO$_4$, 10 mM glucose) to approximately 20% cell density. Ghosts were stored at 4°C for no more than 24 hr prior to sample preparation for the MR experiments.

Ghost Density Calculation, Sample Preparation, and MR

Prior to the MR experiments, the ghosts were washed twice by centrifugation at $12000 \times g$ for 10 min, followed by resuspension in IBES solution. Ghosts were then pelleted by centrifugation at $16000 \times g$ for 10 min, and the supernatant was removed. The extracellular fraction of the pellet was calculated by assaying the concentration of an extracellular marker molecule introduced into the pellet extracellular space. Assays were performed in triplicate. Similar techniques are commonly used to determine extracellular volume fraction in ex vivo brain slices (25). We used FITc-dextran, a fluorescent compound that is inert and unable to cross the cell membrane. Equal volumes (300 μL) of the cell pellet and IBES solution containing FITc-dextran (5 mg/mL, 21.2 kDa average dextran molecular weight) were thoroughly mixed and then centrifuged at $16000 \times g$ for 10 min. A 200-μL sample of the supernatant was taken and its fluorescence compared to a 200-μL standard of 5 mg/ml FITc-dextran standard, using a Bio-Rad VersaFluor fluorimeter (excitation: 490 nm; emission: 520 nm). The dilution of the FITc-dextran solution into the pellet is dependent on the pellet's extracellular fraction.

For studies of cell density, ghost suspensions were prepared by dilution of the pellet with IBES solution to intracellular fractions of 17%, 33%, 50%, and 67%. Three 100-μL samples were prepared at each cell density. To assess the effects of the membrane water channel blocker p-chloromercuribenzenesulphonate (pCMBS), 100 μL of the ghost pellet were mixed with 100 μL of IBES solution to which 2 mM pCMBS had been added. Two pCMBS-treated ghost samples, at an intracellular fraction of 33%, were studied.

To investigate the effects of cell volume change, ghosts were swollen or shrunk by hypo- and hypertonic media. Samples of the ghost pellet (180 μL) were diluted by a 60-μL addition of buffer solution at 0, 150, 300, 450, and 600 mOsm. These hypo- and hypertonic solutions were

prepared by dilution of a ×2 solution (600 mOsm) of IBES solution. On equilibration, the overall osmolarity of the ghost cell suspensions (assuming that ghosts behave as perfect osmometers) were 225 (−25%), 262.5 (−12.5%), 300 (normal), 337.5 (+12.5%), and 375 (+25%) mOsm. In this experiment the measured intracellular fraction of the pellet was 73% ± 3%, so the resultant cell volume change due to the osmolarity of the suspension was expected to alter intracellular fractions to 65%, 55%, 49%, 43%, and 39%, respectively. Three samples of ghost suspensions were prepared at each osmolarity.

Data Acquisition

All NMR data were acquired using a Bruker Instruments Ltd. (Billerica, USA) 750 MHz widebore vertical instrument and console. Samples (approximately 50 μl) were placed in a 25-mm length of 2-mm internal diameter PTFE tubing, which was inserted into a loopgap resonator (3 mm diameter, 8 mm long, in-house construction). Water self-diffusion measurements were acquired using a pulsed gradient spin-echo (PGSE) sequence (26). Experiments were performed at a temperature of 17°C, which was maintained to within 0.5°C by the gradient coil cooling system. Temperature was monitored with a probe thermocouple. Gradient pulses were varied from 0 to 1650 mT/m in 32 equally space steps for diffusion times of 7, 10, 15, and 35 ms, with echo times (TEs) of 15, 18, 25, and 45 ms, respectively. The gradient pulse duration, δ, was 3 ms, the repetition time (TR) was 3 s, and two averages were taken at each *b*-value. Data were acquired into 4096 data points. Signal intensities were determined at each gradient strength by calculating the integral of the water peak from magnitude spectra. Sample T_2 was measured using a Carr-Purcell-Meiboom-Gill (CPMG) sequence (27,28) with a time between echoes of 2 ms, a maximum of 512 echoes, and a TR of 3 s. Only even echoes were used in the data analysis.

Data Analysis

The Levenberg-Marquardt non-linear least-squares fitting routine (29) was employed to fit the biexponential function described by Eq. [1] to signal attenuation with increasing *b*-value.

$$Signal = S_0 \cdot (f_1 \cdot e^{(-bD_1)} + (1 - f_1) \cdot e^{(-bD_2)}) \qquad [1]$$

Values of S_0, f_1, D_1, and D_2 were determined, where S_0 is the signal intensity in the absence of diffusion-weighting gradients, f_1 is the fraction of water with fast ADC, D_1 is the ADC of the fast-diffusing water component, and D_2 is the ADC of the slow-diffusing water component.

A two-compartment exchange model was also fitted to the data. This analysis method (discussed in full detail in Ref. 30) consists of two exchanging tissue compartments. Extracellular diffusion is modulated by tortuosity, intracellular diffusion is modulated by restriction, and water exchanges between intra- and extracellular compartments. The model approximates intracellular restriction by a simple 1D model of restricted diffusion between impermeable parallel planes, and the movement of water molecules
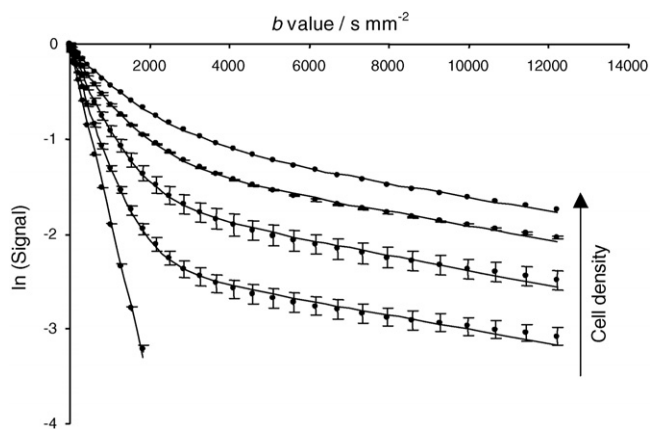

FIG. 1. Mean signal attenuation curves from erythrocyte ghost suspensions at 0%, 17%, 33%, 50%, and 67% density (●), and biexponential fits to these data (—). Data were acquired at a diffusion time of 7 ms. Error bars are ±1 SD.

between intra- and extracellular compartments is described by an exchange rate. This analysis method produces an estimation of intracellular fraction, intra- and extracellular free diffusion coefficients, the dimensions of intracellular diffusion restriction, and the exchange rate between compartments.

RESULTS

Cell Density Variation—Biexponential Analysis

The centrifuged ghost pellet prepared for the cell density studies contained 33% ± 3% extracellular space, as determined by dilution of a fluorescent marker molecule into the extracellular space of the pellet. Thus ghost suspensions with an intracellular fraction of 17%, 33%, 50%, and 67% were examined. Figure 1 shows the logarithm of the signal intensity acquired from the ghost cell suspensions as a function of *b*-value, for ghost samples over this range of cell densities at a diffusion time of 7 ms. All samples demonstrated multiexponential water diffusion, as shown by the nonlinear relationship between log (signal) and *b*-value. Data obtained by fitting a biexponential function to these diffusion profiles are shown in Fig. 2, illustrating the change in f_1, D_1, and D_2.

The fraction of fast-diffusing water, f_1, shows a linear relationship with intracellular fraction. At zero cell density the fast-diffusing fraction comprises all water molecules. f_1 decreases as intracellular fraction increases, indicating an increase in the slow-diffusing water fraction. However, when the data are extrapolated to 100% cell density, f_1 is greater than zero. These data indicate that under these experimental conditions, the slow-diffusing fraction appears smaller than the intracellular fraction.

The ADC of the fast component of the biexponential fit, D_1, is linearly proportional to intracellular fraction, tends toward the ADC of the cell-free buffer as intracellular fraction decreases (approximately 1.8×10^{-3} mm^2 s^{-1} at 17°C), and decreases to a value of about a third that of buffer as intracellular fraction increases to 67%. Extrapolation of this ADC to 100% intracellular fraction yields a
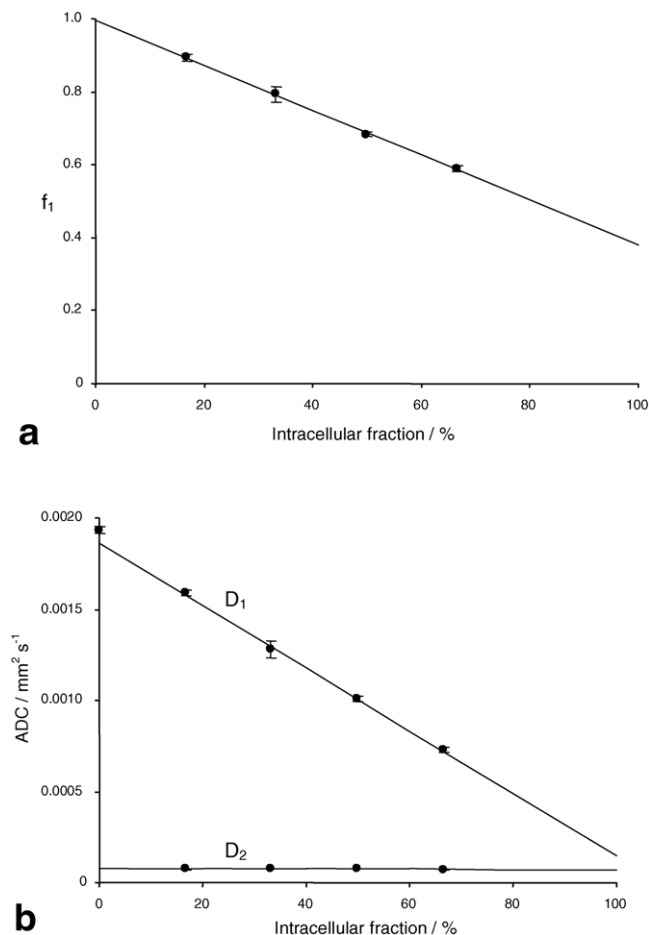
FIG. 2. Biexponential fits to the data shown in Fig. 1, acquired at a diffusion time of 7 ms. **a:** The change in f_1 with intracellular fraction change. **b:** The change in D_1 and D_2 with intracellular fraction change.

diffusion coefficient similar to the ADC of the slow component, D_2.

Water proton T_2 measurements were performed on all samples to ensure that T_2 effects were not responsible for the observed changes in f_1, D_1, and D_2 on cell density change. Samples with an intracellular fraction of 67% had an average T_2 of 340 ms, whereas the cell-free buffer solution had an average T_2 of 790 ms. The estimated T_2 of intracellular water is approximately 220 ms; thus, the effects of T_2 relaxation on signal intensity were assumed to be negligible in these experiments.

Diffusion Restriction of the Slow-Diffusing Component

The ADC of the slow component, D_2, is also affected by cell density, but by a much smaller degree, showing a slight decrease as intracellular fraction increases. The primary factor determining D_2 appears to be restriction of water molecules to the confined dimensions of the intracellular space. The apparent root mean square molecular displacement can be determined from a measured ADC and the diffusion time of the experiment by:

$$r_{app} = \sqrt{6 \cdot T_{diff} \cdot D}. \qquad [2]$$

This measurement determines the average diffusion diameter from a Gaussian distribution of molecular displacements resulting from free diffusion. Applied to the slow component, this measure provides an apparent displacement, r_{app}, as the displacement distribution of intracellular water molecules will deviate from Gaussian due to the restriction boundaries imposed by the cell membrane. Thus r_{app} provides an index of the diffusion restriction imposed by the cell membrane, rather than an absolute measure of cell diameter. This assumes that the water displacement distribution, despite being non-Gaussian, reflects the degree of restriction imposed on water diffusion by the cell dimensions.

Apparent displacement was calculated from the D_2 and T_{diff} for each intracellular fraction and diffusion time in this study. Apparent displacement was similar in all samples, showing a mean value of 1.9 μm with a standard deviation (SD) of 0.2 μm. Erythrocyte ghosts retain the biconcave disc morphology of erythrocytes, which have a thickness of approximately 2 μm and a disc diameter of approximately 8 μm (31).

Transmembrane Water Exchange

Significant water exchange between intra- and extracellular compartments during the diffusion time may result in the observed non-equal relationship between f_1 and extracellular fraction, and the change in D_1 with intracellular fraction. To investigate compartmental exchange effects, ghost suspensions were studied at diffusion times of 7–35 ms. Figure 3a illustrates how the plot of f_1 against cell density changes with increasing diffusion time, the slope of the line decreases indicating that f_1 increases with increasing diffusion time for a given intracellular fraction. We attribute this to the effects of transmembrane water exchange.

The diffusion time-dependent behaviour of the slow component provides an indication of the biophysical origins of the fast and slow components of the biexponential fit. The data suggest that water comprising the slow component is confined to the intracellular space for the duration of the diffusion time, as r_{app} remains unchanged with increasing diffusion time, and the size of this fraction decreases as diffusion time increases (and exchange progresses).

We propose a simple model to explain these observations, similar to the one-way exchange models used to measure membrane permeability in erythrocytes by T_2 measurement, in which the extracellular compartment is doped with a T_2 relaxation agent (21,32). The biexponential analysis separates signal into two components based on the speed of water diffusion. Water molecules that remain in the diffusion-restricted intracellular space for the duration of the diffusion time exhibit a slow ADC, whereas water molecules that reside in the extracellular compartment for part or all of the diffusion time gain an ADC sufficiently faster than the ADC of intracellular water that the biexponential analysis separates signal from these two populations to form the slow and fast-diffusing components, respectively.

Thus the slow component of the biexponential fit originates principally from water that remains in the intracel-
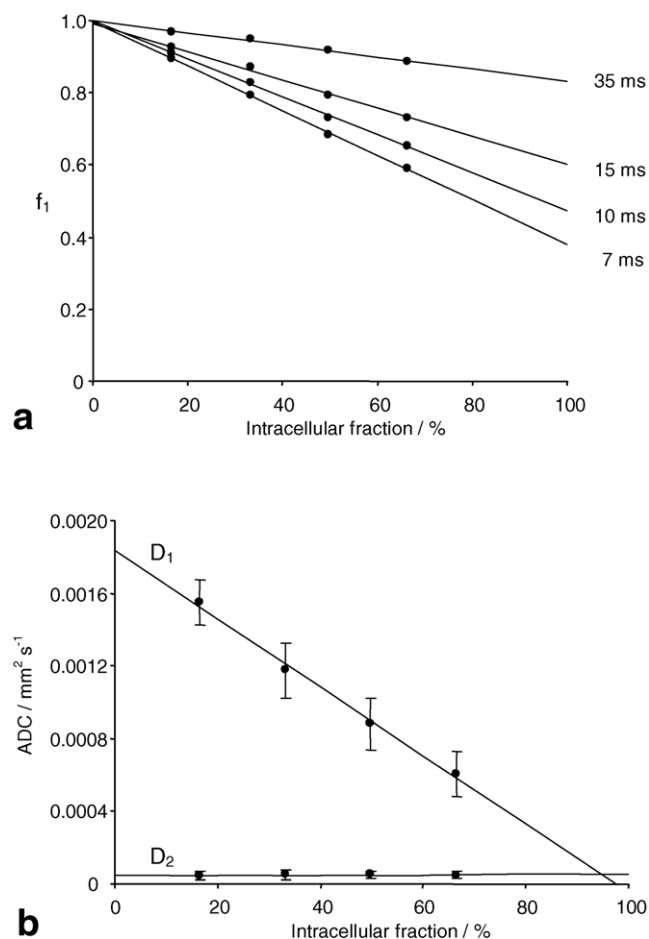
FIG. 3. Biexponential fits to data from erythrocyte ghost suspensions at 17%, 33%, 50%, and 67% intracellular fraction, acquired at diffusion times of 7, 10, 15, and 35 ms. **a:** Dependence of f_1 on intracellular fraction; error bars are within the data point symbols. **b:** Dependence of D_1 and D_2 on intracellular fraction; datapoints are mean values from data acquired at the four diffusion times studied.

lular space for the duration of the diffusion time, and the fast-diffusing component is comprised of water in the extracellular compartment and water molecules that have undergone transmembrane exchange. This is consistent with the observed increase in f_1 with increasing diffusion time, and the decrease in D_1 with increasing intracellular fraction (Fig. 2b). Increasing tortuosity of the extracellular space with increasing intracellular fraction may also be a contributing factor. The value of D_1 at a fixed intracellular fraction showed little change with diffusion time. Values of D_1 and D_2 averaged from 7–35 ms diffusion time measurements are shown in Fig. 3b.

This model dictates that the slow component fraction (f_2, equal to $1 - f_1$) should decrease in size as diffusion time increases, due to the progression of transmembrane water exchange. The rate of transmembrane exchange can be described as the mean residence time or exchange time, T_e, for intracellular water (32). The exchange time describes the exponential rate of decrease in the population of molecules that remains in the intracellular compartment for the duration of the experimental observation time. Pfeuffer

et al. (8,9) incorporated methods similar to those used here to measure water exchange time in perfused F98 glioma cells.

Figure 4 shows plots of f_2 against diffusion time for the four cell density samples studied. Equation [3] describes the exponential decrease of f_2 with diffusion time. Here, f_{in} represents the slow component fraction at a diffusion time of zero, T_{diff} is the experimental diffusion time, and f_2 is the measured slow component fraction.

$$f_2 = f_{in} \cdot e^{\frac{-T_{diff}}{T_e}}$$ [3]

The exchange time, T_e, describes the rate at which diffusion restricted intracellular water molecules leave the cell and acquire an elevated ADC. Equation [3] was fitted to these data and a value of T_e was determined from each diffusion time measurement of each sample studied. The mean intracellular residence time was 21.9 ± 1.3 ms. This is in good agreement with measurements made by MRS T_2 doping methods which reported a T_e of 19–17 ms for human erythrocyte ghosts at 15–20°C (21). Values of f_{in} and the other biophysical properties of the ghost suspensions determined by the biexponential analyses are shown in Table 1.

Effects of a Membrane Water Channel Blocker

Ghost membrane water permeability was reduced by addition of pCMBS to the suspension solution. pCMBS binds to aquaporin water channels (21), reducing the rate of water exchange. Figure 5 shows the logarithm of signal intensity against *b*-value for 33% density ghosts in the presence and absence of pCMBS, acquired at a diffusion time of 7 ms. The addition of pCMBS results in reduced signal attenuation at high *b*-values, and fitting a biexponential function to these data demonstrated a 33% larger slow-diffusing component in the pCMBS-treated sample at
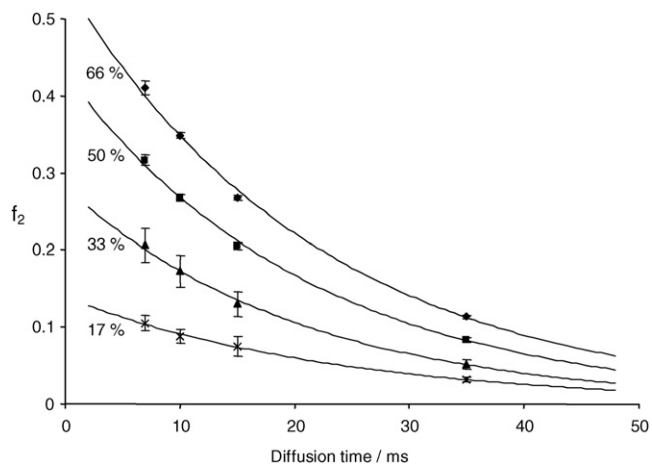

FIG. 4. The fraction of the slow component, f_2, against diffusion time for the four intracellular fractions studied. The exponential decrease in the size of f_2 is attributed to transmembrane water exchange. The exchange time, T_e, calculated from these curves was 22.1, 21.2, 20.5, and 23.7 ms for the 66%, 50%, 33%, and 17% intracellular fraction samples, respectively. The mean value of T_e from all samples was 21.9 ± 1.3 ms.

Table 1
Results of Biexponential Analysis and Two Compartment Exchange Analysis to Multiple Diffusion Time Datasets*

Cell density	Biexponential analysis at multiple diffusion times					Two compartment exchange model				
	f_{intra}	D_{extra} $(10^{-3}$ mm^2 s$^{-1})$	D_{intra} $(10^{-3}$ mm^2 s$^{-1})$	Mean cell diameter/μm	T_e/ms	f_{intra}	D_{extra} $(10^{-3}$ mm^2 s$^{-1})$	D_{intra} $(10^{-3}$ mm^2 s$^{-1})$	Mean cell diameter/μm	T_e/ms
67%	0.55 ± 0.01	0.73 ± 0.02	0.071 ± 0.002	1.9 ± 0.2	22.1 ± 0.3	0.58	2.01	n/a	3.6	11.9
50%	0.43 ± 0.01	1.01 ± 0.01	0.076 ± 0.001	2.0 ± 0.1	21.2 ± 0.3	0.44 ± 0.02	1.95 ± 0.1	n/a	2.4 ± 0.1	10.5 ± 0.3
33%	0.28 ± 0.03	1.27 ± 0.05	0.079 ± 0.001	1.9 ± 0.1	20.5 ± 0.2	0.29 ± 0.03	1.88 ± 0.1	n/a	2.5 ± 0.2	10.0 ± 0.7
17%	0.14 ± 0.01	1.37 ± 0.01	0.074 ± 0.001	1.7 ± 0.2	23.7 ± 0.4	0.14	1.83	n/a	2.7	16.1
33% + 2mM pCMBS	0.32	1.39	0.052	1.6	44.9	0.29	1.9	n/a	2.2	25

*The intracellular fraction measurements determined by biexponential analysis were calculated by extrapolating data to zero diffusion time. D_{fast} and D_{slow} represent ADCs determined by biexponential analysis of data acquired at a diffusion time of 7 ms. Results from two compartment exchange analysis were excluded if $\chi^2 > 5$, hence the results represent n = 3 for 50% and 33% intracellular fraction samples, and n = 2 for all other samples.
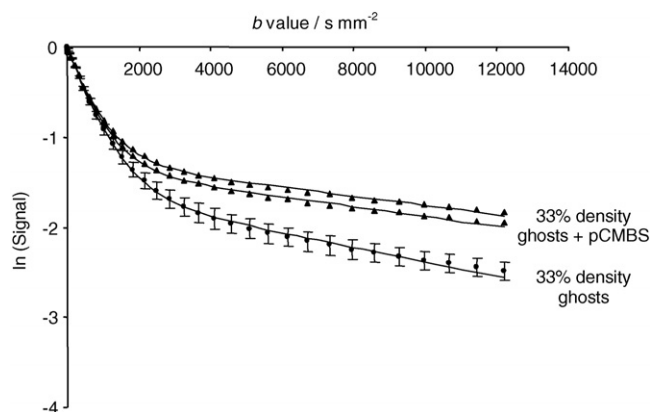

FIG. 5. Mean signal attenuation curves from erythrocyte ghost suspensions at 33% intracellular fraction, in the presence (▲, $N = 2$) and absence (●, $N = 3$; error bars are ±1 SD) of 2 mM pCMBS. Data were acquired at a diffusion time of 7 ms.

a diffusion time of 7 ms, consistent with reduced transmembrane exchange (data not shown). The exchange time was calculated from biexponential fits to data acquired at diffusion times of 7, 10, 15, and 35 ms, as described above (data not shown). The two pCMBS-treated ghost samples had a mean intracellular residence time of 43 and 47 ms, twice that of pCMBS-free ghosts. The biexponential fit data also allowed calculation of the apparent displacement of water molecules comprising the slow-diffusing fraction, yielding a mean r_{app} of 1.6 μm, close to that determined in pCMBS-free ghosts.

Two-Compartment Exchange Model

Diffusion data were analysed using a two-compartment exchange model based on a previously-described model (30). Table 1 shows the results of fitting this model to the diffusion data. Fits were rejected if the χ^2 value was larger than 4 (normalised), and acceptable fits had χ^2 values of approximately 0.8–1.4. Hence the results represent $N = 3$ for 50% and 33% intracellular fraction samples, and $N = 2$ for all other samples.

The calculated intracellular fractions agree well with the assayed intracellular fractions, and the diffusion coefficient of extracellular water is approximately that of water in cell-free buffer solution for all cell densities, indicating that the analysis accounts for extracellular tortuosity and exchange effects. The intracellular diffusion coefficient could not be determined from these diffusion data, indicating that in these ghost samples the rate of intracellular water diffusion is determined by restriction dimensions rather than intracellular viscosity.

The calculated cell size is larger than the apparent displacement determined by the biexponential analysis method: 2.8 ± 0.8 μm. In this analysis, intracellular restriction is approximated by a 1D model of restriction between impermeable planes, whereas the biexponential method assumes a Gaussian distribution of molecular displacements from their origins. Neither of these model assumptions accurately describes the 3D morphology of an erythrocyte ghost, and improved modelling procedures may be required to account for this in analysis methods.

Cell Swelling and Shrinkage

Figure 6 shows the logarithm of the signal intensity acquired from the ghost cell suspensions at increasing b-value for five groups of ghost samples at hypo-, iso-, or hypertonic conditions, acquired at a diffusion time of 7 ms. Ghost samples under hypotonic conditions show increased signal at high b-values relative to isotonic samples, as expected for an increase in intracellular fraction due to cell swelling. Samples under hypertonic conditions show decreased signal at high b-values, as expected for cell shrinkage.

Figure 7 shows the results of biexponential analysis applied to these data. The fast component fraction, f_1, decreases as the cells swell and increases as the cells shrink. There is a linear relationship between extracellular fraction and f_1, although f_1 is not equal to extracellular fraction. The ADCs of the fast and slow components, D_1 and D_2, decrease as cell volume (and therefore intracellular fraction) increases. Again, the trend in D_2 is much smaller than that of D_1. The slight decrease in D_2 with cell swelling seems unexpected, as the size of the diffusion restricted compartment is increasing; however, this shift in D_2 is also seen with cell density increase where the cell size remains constant. Thus a likely explanation for this shift is the imperfect separation of intracellular water from extracellular and mixing water by the (underparameterised) biexponential fitting routine, rather than a decrease in diffusion restriction. Such decreases in the biexponential fast- and slow-component ADCs were observed on cell swelling in rat brain in vivo in studies performed by Niendorf et al. (3).

DISCUSSION

Several groups have used model systems composed of cell suspensions to study water diffusion in biological systems. Latour et al. (33) studied erythrocyte suspensions at a range of haematocrits to investigate the tortuosity of the extracellular diffusion path and effects of membrane permeability on ADC measurements. Li and Stanisz (30) and Stanisz et al. (34) further developed studies of erythrocyte

FIG. 7. Biexponential fits to the data shown in Fig. 6. **a:** The change in f_1 on intracellular fraction change, effected by cell swelling or shrinkage. **b:** The concomitant change in D_1 and D_2 on intracellular fraction change.

suspensions by developing an analytical model of human blood, describing compartmental dynamics and water signal attenuation in terms of diffusion and relaxation. Other studies have applied analytical models to cultured neuronal cells (8,9), a tissue type that is physiologically more relevant to the brain in vivo and may be used to assess the effects of physiologically relevant insults on the diffusion properties of water. In the present study we employed an analytical model incorporating restricted intracellular water diffusion at permeable boundaries, which appeared to well describe the diffusion processes in this system.

Recent studies have demonstrated multiexponential water diffusion in perfused hippocampal brain slices (6,12,13). Fitting to a two-compartment (biexponential) model generated fast- and slow-diffusing water components that, as a first approximation, were attributed to the extra- and intracellular compartments, respectively. Hypotonic insult and ouabain- or NMDA-induced cell swelling resulted in an increase in the fraction of water with low ADC. The ADCs of the fast and slow components remained unchanged. The size of the fraction change on insult correlated with the expected change in cell volume; however, the ratio of fast- to slow-diffusing water was not equal to
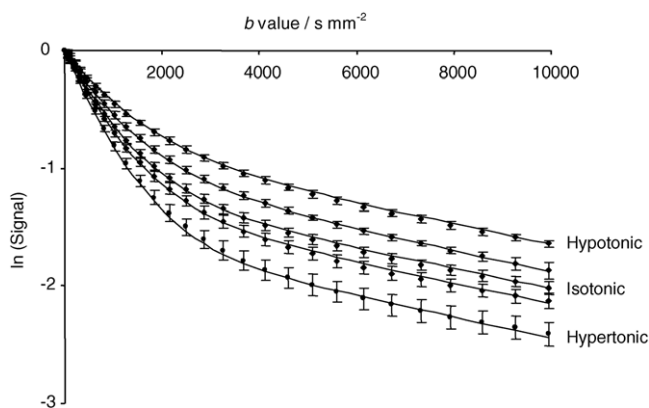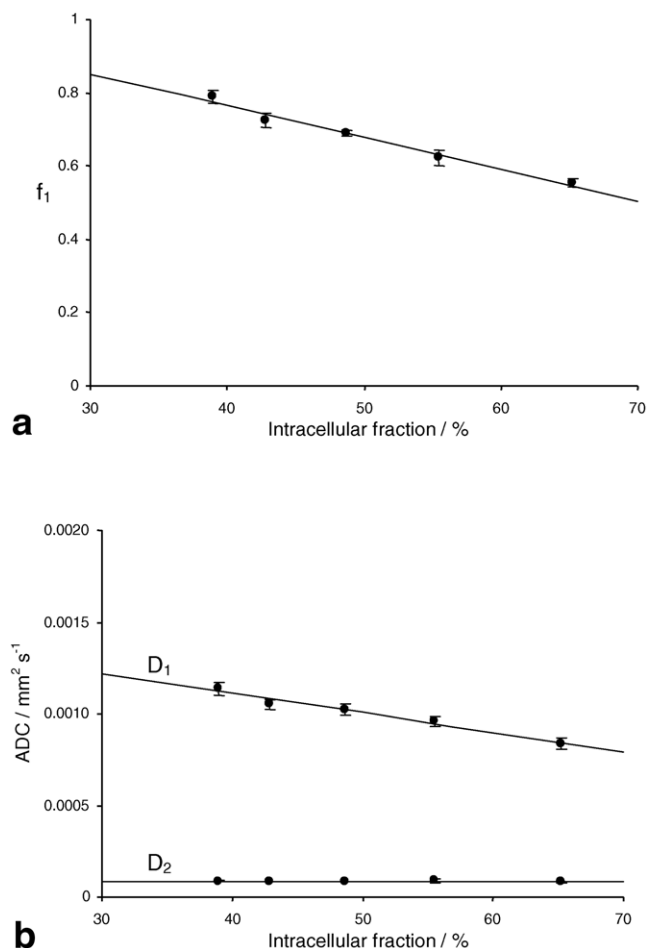
FIG. 6. Signal attenuation curves from erythrocyte ghost suspensions under 25% and 12.5% hypotonic, isotonic, and 25% and 12.5% hypertonic conditions (●); biexponential fits to these data (—). Error bars are ±1 SD.

the ratio of extra- to intracellular water. This discrepancy was attributed to T_2 differences between intra- and extracellular compartments. An alternative explanation could be significant exchange between the intra- and extracellular compartments, or the presence of fast-diffusing water in the intracellular compartment. Diffusion-weighted microimaging studies of single isolated *Aplysia* neurons demonstrated non-monoexponential water diffusion in the cytoplasm alone (19), suggesting that the biexponential model may poorly describe water diffusion in a cellular system.

In this study we developed a tissue model to explore the effects of biophysical tissue properties on multiexponential water diffusion. The data demonstrated non-monoexponential water diffusion. As a first approximation to describe the model tissue, the data were fit to a two-compartment (biexponential) model. A two-compartment exchange model was also employed, and the results of the analysis methods were compared. The biexponential fit was underparameterised, as it was unable to account for the significant water exchange between the intra- and extracellular compartments. However, by measuring and altering the intracellular fraction and performing diffusion measurements at a range of diffusion times, we were able to interpret the diffusion data. We demonstrated that the fast component of the biexponential fit appears linearly proportional to cell density at the diffusion times studied, which allows the changes in cell density to be tracked. The slow component of the fit appeared to originate from water restricted solely to the intracellular compartment, with its ADC reflecting the dimensions of the cell. There was a diffusion time-dependent decrease in the fraction of water with a slow ADC. Measuring the rate that f_2 changed with increasing diffusion time allowed for the calculation of the mean intracellular residence time, which was shown to increase when membrane permeability to water was decreased. Extrapolating the measurement of slow-component fraction to a diffusion time of zero provided an estimation of intracellular fraction in the limit of slow exchange.

The two-compartment exchange model successfully determined intracellular fraction and accounted for the effects of tortuosity and exchange in the extracellular compartment. The mean intracellular residence time determined from this analysis was 12 ± 4 ms. This is considerably shorter than the value determined by the biexponential method, which may be due in part to the difference in restriction geometries assumed by the two models. Further modelling and simulation studies are required, and will form the basis of future studies. Nonetheless, both analysis methods proved to be effective at tracking changes in exchange time when membrane permeability was altered. Both analyses showed that mean intracellular residence time increased by a factor of two when pCMBS was added to the ghost suspension.

Intracellular fractions calculated by the two analysis methods were consistent, but they were lower than the intracellular fraction determined by fluorescence assay. This may reflect inaccuracy in the assay method, or inadequacy of our analysis methods to determine intracellular fraction by diffusion analysis. The assay method was checked by measuring the water content of a glass bead/ water mix, and it was accurate to $\pm 1\%$. Thus the discrepancy between assayed and calculated intracellular fraction warrants further investigation.

The strength of the erythrocyte ghost model lies in our ability to individually perturb specific biophysical properties and observe the effects in the MR properties of the ghost suspension. Although the tissue is far removed from, for example, neural tissue, the model demonstrates response to perturbations analogous to those seen in vivo. Niendorf et al. (3) monitored the change in the water diffusion properties of brain tissue water on cerebral ischemia in rats. Biexponential analysis indicated a decrease in the ADC of both fast- and slow-diffusing water components and a decrease in f_1 on ischemic insult. These changes occurred concurrently with cell swelling, as monitored by electrical impedance measurements. Our data demonstrate a similar shift in the diffusion properties of water on increase in intracellular fraction due to ghost cell density change or ghost volume increase. Erythrocyte ghosts provide a model that is obviously far removed from mammalian brain tissue: the extracellular compartment is saline, and the intracellular compartment is saline-filled. Membrane permeability to water is much higher than that found in neural cells due to the presence of water channel proteins in the erythrocyte membrane (21). However, the observed changes in the diffusion profile follow the same trends in the ghost cell model as seen in vivo. Both analysis methods employed to interpret the diffusion data were effective at tracking changes in cell density and membrane permeability. We plan to develop our analysis methods to more accurately represent the biophysical parameters of the ghost model and neuronal tissues to provide more appropriate analyses of experimental data, and aid extrapolation of results to neuronal tissue models.

Biexponential analysis has been used on a range of tissues and tissue models by other groups (3,12,16,17). Although it is clear that the biexponential fitting without exchange is inappropriate for the erythrocyte ghost system at the diffusion time used, our analysis shows that trends in the fits may be interpreted to reflect microstructural changes. For some biological systems the biexponential model may be appropriate, for example in tissues with larger cells (e.g., some regions of brain tissue) and/or where the diffusion rates are slower and/or where the diffusion time is reduced. The biexponential fit may also be more appropriate than more complex analysis methods when data are noise-limited and, consequently, complex fits are not robust. Nevertheless, the results of a simple biexponential analysis must be interpreted with care.

The complexity of real tissues and the inherently poor sensitivity of MR mean that real biological systems most likely can never be accurately modelled with realistic (complex) fitting procedures. However, it is clear that both of the simplistic mathematical modelling approaches employed here were successful at tracking changes in the MR signals that were representative of real biophysical changes. Thus, suitable (if simplistic) modelling procedures may provide insights into the mechanisms of signal changes observed in real tissues, thereby aiding in improving the clinical sensitivity and specificity of diffusion MRI.

CONCLUSIONS

The erythrocyte ghost model was developed to provide a simple, controllable, flexible model for the study of compartmentation effects on the MR signal from biological tissues. Ghost cell suspensions demonstrated non-mono-exponential water diffusion. A biexponential fit resolved fast- and slow-diffusing water components. However, these components did not directly correspond to extra- and intracellular compartments. The data suggest that a biexponential fit to this system is underparameterised, because water exchange between intra- and extracellular compartments was significant. However, biexponential analysis tracked changes in cell density and cell size, and provided an index of intracellular water residence time and intracellular restriction dimensions. The biophysical origins of the fast- and slow-diffusing components of the fit were proposed for this model system. Biexponential analysis is inappropriate for this system because of compartmental water exchange, but it may prove adequate for tissues in which water exchange between compartments is in the slow regime, i.e., tissues with large cells, low membrane permeability to water, slower diffusion rates, and/or shorter experimental diffusion times.

The two-compartment exchange model provided a more appropriate analysis compared to the standard biexponential method; however, the calculated mean intracellular residence time and cell dimensions were lower than expected. Future studies will develop analysis methods to better describe the biophysical properties of tissues and aid in the translation of these studies to in vivo and clinical situations.

REFERENCES

1. Busza AL, Allen KL, King MD, van Bruggen N, Williams SR, Gadian DG. Diffusion-weighted imaging studies of cerebral ischemia in gerbils—potential relevance to energy failure. Stroke 1992;23:1602–1612.
2. Norris DG, Niendorf T, Leibfritz D. Healthy and infarcted brain tissues studied at short diffusion times: the origins of apparent restriction and the reduction in apparent diffusion coefficient. NMR Biomed 1994;7:304–310.
3. Niendorf T, Dijkhuizen RM, Norris DG, van Lookeren C, Nicolay K. Biexponential diffusion attenuation in various states of brain tissue: implications for diffusion-weighted imaging. Magn Reson Med 1996;36:847–857.
4. Szafer A, Zhong J, Gore JC. Theoretical model for water diffusion in tissues. Magn Reson Med 1995;33:697–712.
5. Duong TQ, Ackerman JJ, Ying HS, Neil JJ. Evaluation of extra- and intracellular apparent diffusion in normal and globally ischemic rat brain via 19F NMR. Magn Reson Med 1998;40:1–13.
6. Blackband SJ, Bui JD, Buckley DL, Zelles T, Plant HD, Inglis BA, Phillips MI. MR microscopy of perfused brain slices. Magn Reson Med 1997;38:1012–1015.
7. Verheul HB, Balazs R, Berkelbach van der Sprenkel JW, Tulleken CA, Nicolay K, Tamminga KS, van Lookeren C. Comparison of diffusion-weighted MRI with changes in cell volume in a rat model of brain injury. NMR Biomed 1994;7:96–100.
8. Pfeuffer J, Flogel U, Dreher W, Leibfritz D. Restricted diffusion and exchange of intracellular water: theoretical modelling and diffusion time dependence of 1H NMR measurements on perfused glial cells. NMR Biomed 1998;11:19–31.
9. Pfeuffer J, Flogel U, Leibfritz D. Monitoring of cell volume and water exchange time in perfused cells by diffusion-weighted 1H NMR spectroscopy. NMR Biomed 1998;11:11–18.
10. Stanisz GJ, Szafer A, Wright GA, Henkelman RM. An analytical model of restricted diffusion in bovine optic nerve. Magn Reson Med 1997;37:103–111.
11. Forder JR, Bui JD, Buckley DL, Blackband SJ. MR imaging measurement of compartmental water diffusion in perfused heart slices. Am J Physiol Heart Circ Physiol 2001;281:H1280–H1285.
12. Buckley DL, Bui JD, Phillips MI, Zelles T, Inglis BA, Plant HD, Blackband SJ. The effect of ouabain on water diffusion in the rat hippocampal slice measured by high resolution NMR imaging. Magn Reson Med 1999;41:137–142.
13. Bui JD, Buckley DL, Phillips MI, Blackband SJ. Nuclear magnetic resonance imaging measurements of water diffusion in the perfused hippocampal slice during N-methyl-D-aspartate-induced excitotoxicity. Neuroscience 1999;93:487–490.
14. Stanisz GJ, Henkelman RM. Diffusional anisotropy of T_2 components in bovine optic nerve. Magn Reson Med 1998;40:405–410.
15. Henkelman RM, Stanisz GJ, Kim JK, Bronskill MJ. Anisotropy of NMR properties of tissues. Magn Reson Med 1994;32:592–601.
16. Mulkern RV, Gudbjartsson H, Westin CF, Zengingonul HP, Gartner W, Guttmann CR, Robertson RL, Kyriakos W, Schwartz R, Holtzman D, Jolesz FA, Maier SE. Multi-component apparent diffusion coefficients in human brain. NMR Biomed 1999;12:51–62.
17. Mulkern RV, Zengingonul HP, Robertson RL, Bogner P, Zou KH, Gudbjartsson H, Guttmann CR, Holtzman D, Kyriakos W, Jolesz FA, Maier SE. Multi-component apparent diffusion coefficients in human brain: relationship to spin-lattice relaxation. Magn Reson Med 2000;44:292–300.
18. Szafer A, Zhong J, Anderson AW, Gore JC. Diffusion-weighted imaging in tissues: theoretical models. NMR Biomed 1995;8:289–296.
19. Grant SC, Buckley DL, Gibbs S, Webb AG, Blackband SJ. MR microscopy of multiple component water diffusion in isolated single neurons. Magn Reson Med 2001;46:1107–1112.
20. Pfeuffer J, Provencher SW, Gruetter R. Water diffusion in rat brain in vivo as detected at very large *b* values is multicompartmental. MAGMA 1999;8:98–108.
21. Benga G, Pop VI, Popescu O, Borza V. On measuring the diffusional water permeability of human red blood cells and ghosts by nuclear magnetic resonance. J Biochem Biophys Methods 1990;21:87–102.
22. Maier CF, Paran Y, Bendel P, Rutt BK, Degani H. Quantitative diffusion imaging in implanted human breast tumors. Magn Reson Med 1997;37:576–581.
23. Lyng H, Haraldseth O, Rofstad EK. Measurement of cell density and necrotic fraction in human melanoma xenografts by diffusion weighted magnetic resonance imaging. Magn Reson Med 2000;43:828–836.
24. Wood PG. Preparation of white resealable erythrocyte ghosts. Methods Enzymol 1987;149:271–280.
25. Law RO. Taurine efflux and the regulation of cell volume in incubated slices of rat cerebral cortex. Biochim Biophys Acta 1994;1221:21–28.
26. Stejskal EO, Tanner JE. Spin diffusion measurements: spin echos in the presence of a time-dependent field gradient. J Chem Phys 1965;42:3597–3603.
27. Carr HY, Purcell EM. Effects of diffusion on free precession in nuclear magnetic resonance experiments. Phys Rev 1954;94:630–638.
28. Meiboom S, Gill D. Modified spin-echo method for measuring nuclear relaxation times. Rev Sci Instr 1958;29:688–691.
29. Marquardt DW. An algorithm for least-squares estimation of nonlinear parameters. J Soc Ind Appl Math 1963;11:431–441.
30. Li JG, Stanisz GJ, Henkelman RM. Integrated analysis of diffusion and relaxation of water in blood. Magn Reson Med 1998;40:79–88.
31. Weinstein RS. The morphology of adult red cells. In: Surgenor DM, editor. The red blood cell. New York: Academic Press; 1974. p 213–268.
32. Herbst MD, Goldstein JH. A review of water diffusion measurement by NMR in human red blood cells. Am J Physiol 1989;256:C1097–C1104.
33. Latour LL, Svoboda K, Mitra PP, Sotak CH. Time-dependent diffusion of water in a biological model system. Proc Natl Acad Sci USA 1994;91:1229–1233.
34. Stanisz GJ, Li JG, Wright GA, Henkelman RM. Water dynamics in human blood via combined measurements of T_2 relaxation and diffusion in the presence of gadolinium. Magn Reson Med 1998;39:223–233.